

Can steady-state Schrödinger cats survive in subharmonic generation with anharmonic nonlinearities?

Feng-Xiao Sun,^{1, 2, 3, 4} Qiongyi He,^{1, 2, 5,*} Qihuang Gong,^{1, 2, 5} Run Yan Teh,³ Margaret D. Reid,^{3, 4} and Peter D. Drummond^{3, 4}

¹*State Key Laboratory for Mesoscopic Physics and Collaborative Innovation Center of Quantum Matter, School of Physics, Peking University, Beijing 100871, China*

²*Collaborative Innovation Center of Extreme Optics, Shanxi University, Taiyuan, Shanxi 030006, China*

³*Centre for Quantum and Optical Science, Swinburne University of Technology, Melbourne 3122, Australia*

⁴*Institute of Theoretical Atomic, Molecular and Optical Physics (ITAMP), Harvard University, Cambridge, Massachusetts 02138, USA*

⁵*Beijing Academy of Quantum Information Sciences, West Bld. #3, No.10 Xibeiwang East Rd., Haidian District, Beijing 100193, China*

We discuss general properties of the equilibrium state in superconducting quantum circuits with anharmonic nonlinearities and detunings, in the nonlinear regime. By comparing moments of the steady state and those of a Schrödinger cat, we show that true Schrödinger cats cannot survive in the steady state if there is a single-photon loss. A delta-function ‘cat-like’ steady-state distribution can be formed, but this only exists in the limit of extremely large nonlinearity. In general, the steady state is a mixed state whose purity is reduced by driving.

The Schrödinger cat is a famous thought experiment of E. Schrödinger [1], where a cat is placed in a quantum superposition of two macroscopically distinct states, either alive or dead. It opens the fundamental question of whether quantum theory holds true in the macroscopic world [2–4]. A common strategy for Schrödinger cats [5] is via non-equilibrium subharmonic generation [6, 7] leading to discrete time symmetry-breaking or time crystals [8]. Macroscopic superposition states have been proposed in quantum computation [9], quantum teleportation [10], quantum metrology [11] and quantum key distribution [12]. They have also been experimentally realized in atoms [13, 14] and photons [15].

The steady state of above-threshold subharmonic generation is known for parametric down-conversion without anharmonicities or detuning [6, 16]. In this case transient Schrödinger cats are possible [5, 17, 18]. Quantum subharmonic generation with anharmonic nonlinearities has been achieved in superconducting circuits [19]. Relatively large cat states were observed. In the experiment, the physics of the quantum steady state is different from previous studies [20]. This raises the question of the exact steady state limit as an example of how dissipation restores broken time symmetry, with applications to solving combinatorial optimization problems [21].

Quantum optical and quantum circuit physics are similar except that quantum circuits operate at microwave instead of optical frequencies. General driven quantum subharmonic generation with damping and weak nonlinearities was studied in a previous paper [20], where non-equilibrium quantum tunneling [22] occurs. Here we focus on the cat-like properties of the steady states in the case of strong combined parametric and anharmonic

nonlinearities, as found in recent experiments.

We analytically calculate the exact steady state in subharmonic generation with strong parametric and anharmonic nonlinearities, and use the resulting correlation function to show that neither simple mixtures of coherent states nor Schrödinger cat states can occur in the steady state. We also expect this behavior in more complex time-crystal experiments. Although a steady-state mixture of coherent states [16] is achievable as a limiting case of extremely strong nonlinearities, it is still a mixed state. This is consistent with the superconducting experiment [19] where an approximate Schrödinger cat was observed in a transient regime. The steady-state in the zero loss case is not uniquely defined, due to conserved number parity.

Firstly, we summarize the system properties and theoretical techniques used previously [7, 20, 23], and then treat the detailed properties of the strongly coupled case. The annihilation and creation operators of the k -th mode in two coupled resonant cavities are a_k, a_k^\dagger at frequencies ω_k . They have a non-interacting Hamiltonian in the rotating frame of $H_0 = \hbar \sum \Delta_k a_k^\dagger a_k$, where $\Delta_k = \omega_k - k\omega_0 \ll \omega_0$ for an input laser frequency of $2\omega_0$. The interaction Hamiltonian is then given by

$$H_I = \hbar \frac{\chi}{2} a_1^\dagger a_1^2 + \left(i\hbar \frac{\kappa}{2} a_2 a_1^\dagger + i\hbar \mathcal{E}_2 a_2^\dagger + h.c. \right). \quad (1)$$

Here \mathcal{E}_2 is the envelope amplitude of the driving for the mode a_2 , and κ, χ are the parametric and anharmonic nonlinearities [24] respectively. Anharmonic nonlinearities are only included for the mode a_1 .

In addition, we include single-photon and two-photon losses in this open system. Defining $H = H_0 + H_I$, the master equation for the density matrix ρ is

$$\dot{\rho} = -\frac{i}{\hbar} [H, \rho] + \sum_{k,j>0} \frac{\gamma_k^{(j)}}{j} \mathcal{L}_k^{(j)} [\rho]. \quad (2)$$

* qiongyihe@pku.edu.cn

Here $\gamma_k^{(j)}$ are the relaxation rates for j -photon losses in the k -th mode, with no two-photon losses in mode $k = 2$ for simplicity. The dissipative terms are

$$\mathcal{L}_k^{(j)}[\rho] = 2\hat{O}\rho\hat{O}^\dagger - \rho\hat{O}^\dagger\hat{O} - \hat{O}^\dagger\hat{O}\rho, \quad (3)$$

where $\hat{O} = \hat{a}_k^j$. The corresponding thermal noises are set to zero. This allows us to study the steady-state properties in the low-temperature limit, in order to understand this exactly soluble case of maximal quantum coherence.

We suppose the second harmonic mode is strongly damped, as in the recent Yale experiments [19]. Complex single-photon loss terms are defined as $\gamma_k = \gamma_k^{(1)} + i\Delta_k$. An adiabatic Hamiltonian is obtained for $a \equiv a_1$ as:

$$\frac{H_A}{\hbar} = \Delta_1 a^\dagger a + i \left[\frac{\epsilon}{2} a^{\dagger 2} - h.c. \right] + \frac{\chi_e}{2} a^{\dagger 2} a^2, \quad (4)$$

The effective driving field ϵ and nonlinearity χ_e are:

$$\epsilon = \frac{\kappa}{\gamma_2} \mathcal{E}_2, \quad \chi_e = \chi - \frac{\Delta_2}{2} \left| \frac{\kappa}{\gamma_2} \right|^2. \quad (5)$$

The master equation of the reduced density matrix $\rho_1 = \text{Tr}_2(\rho)$ is then obtained as

$$\begin{aligned} \frac{\partial}{\partial t} \rho_1 &= \frac{1}{i\hbar} [H_A, \rho_1] + \gamma_1^{(1)} (2a\rho_1 a^\dagger - a^\dagger a\rho_1 - \rho_1 a^\dagger a) \\ &+ \frac{\gamma_e^{(2)}}{2} (2a^2 \rho_1 a^{\dagger 2} - a^{\dagger 2} a^2 \rho_1 - \rho_1 a^{\dagger 2} a^2), \end{aligned} \quad (6)$$

with an effective two-photon loss $\gamma_e^{(2)}$, where

$$\gamma_e^{(2)} = \gamma_1^{(2)} + \frac{\gamma_2^{(1)}}{2} \left| \frac{\kappa}{\gamma_2} \right|^2. \quad (7)$$

We introduce a generalized P-representation [25] to obtain the exact solution to the steady-state. If we expand the reduced quantum density matrix in terms of coherent state projection operators and a complex P-distribution $P(\alpha, \alpha^+, t)$, one then obtains

$$\hat{\rho}_1 = \oint d\alpha d\alpha^+ P(\alpha, \alpha^+) \frac{|\alpha\rangle\langle\alpha^{+*}|}{\langle\alpha^{+*}|\alpha\rangle}, \quad (8)$$

where $|\alpha\rangle$ is a coherent state and $d\alpha d\alpha^+$ is a surface integral measure over a closed surface, so that boundary terms will vanish on integration by parts. The adiabatic Hamiltonian results in a single-mode Fokker-Planck equation for P ,

$$\frac{\partial P}{\partial t} = \left\{ \frac{\partial}{\partial \alpha} [\gamma\alpha - \varepsilon(\alpha)\alpha^+] + \frac{1}{2} \frac{\partial^2}{\partial \alpha^2} \varepsilon(\alpha) + h.c. \right\} P, \quad (9)$$

where we define $\gamma \equiv \gamma_1$ and $\varepsilon(\alpha) = \epsilon - g\alpha^2$. We also introduce an effective complex nonlinear decay of $g = \gamma_e^{(2)} + i\chi_e$. The notation *h.c.* indicates hermitian conjugate terms obtained by the replacement of $\alpha \rightarrow \alpha^+$, and the conjugation of all complex parameters [20].

The steady-state solution of the Fokker-Planck equation (9) can then be derived with the potential equations [26–29], $P(\alpha, \alpha^+) = N \exp[-\Phi(\alpha, \alpha^+)]$, where N is a normalization constant and the steady-state potential solution is

$$\Phi(\alpha, \alpha^+) = -2\alpha^+ \alpha - c \ln[\lambda_c - \alpha^2] - c^* \ln[\lambda_c^* - \alpha^{+2}], \quad (10)$$

with dimensionless parameters $c = \gamma/g - 1$ and $\lambda_c = \epsilon/g$. Thus, the steady-state probability distribution is

$$P(\alpha, \alpha^+) = N(\lambda_c - \alpha^2)^c (\lambda_c^* - \alpha^{+2})^{c^*} e^{2\alpha^+ \alpha}. \quad (11)$$

This is the exact zero-temperature steady-state solution for the density matrix. All the parameters here can have complex values, which is necessary when treating the situations in recent quantum circuit experiments [19].

Now we will consider the relevant parameters in the experiment [19]. In our notation, we obtain the parameters as $\gamma/2\pi = 3.98\text{kHz}$, $g/2\pi = (7.96 + 4i)\text{ kHz}$ and $\epsilon = (-19.2 - 0.07i)\text{ kHz}$. Thus we have $c = -0.6 - 0.2i$ and $\lambda_c = -1.93 + 0.96i$. Since the real part of c is negative, there will be singularities occurring at $\alpha = \pm\sqrt{\lambda_c}$ or $\alpha^+ = \pm\sqrt{\lambda_c^*}$.

From now on, we will treat the strong coupling regime, which corresponds to the parameter region of $\text{Re}(c) < 0$. Using the definitions of c and g , we have

$$c = \frac{(\gamma_1^{(1)} + i\Delta_1)(\gamma_e^{(2)} - i\chi_e)}{|g|^2} - 1. \quad (12)$$

Hence, $\text{Re}(c) < 0$ is equivalent to $\gamma_e^{(2)}(\gamma_1^{(1)} - \gamma_e^{(2)}) + \chi_e(\Delta_1 - \chi_e) < 0$. This is satisfied if there is either a weak single-photon damping $\gamma_1^{(1)}$ or strong nonlinear couplings $\chi_e, \gamma_e^{(2)}$. It is easily checked, provided there are no detunings, that $\text{Re}(c) \geq -1$ and the limit $c \rightarrow -1$ occurs if $\gamma_1^{(1)} \ll \gamma_e^{(2)}$ or $\gamma_1^{(1)} \ll \chi_e$. Considering nonlinear losses are always weak, the relation $\gamma_1^{(1)} \ll \gamma_e^{(2)}$ can occur with large κ refer to Eq. (7). Thus the limit $c \rightarrow -1$ occurs either with large nonlinearities κ or χ .

Due to the negative powers c , there are cuts on the complex integration manifold, and corresponding branch points that describe a topological structure, rather than local potential minima. This is why there is no quantum tunneling, although transient Schrödinger cats can be formed in this type of experiment [19]. This is a completely different manifold to that investigated in the previous work [20], where the real part of c is positive and there is quantum tunneling between local potential minima on a finite, bounded manifold. To define the distribution, we must choose complex integration contours which are closed and continuous [7, 23, 25]. This is obtained from inserting a cut between the branch-points combined with complex Pochhammer contours, as used to represent the beta and hypergeometric functions [30–32].

We will use these exact analytic results to check the validity of approximate delta-function steady-state distributions which we introduce later (18), via the second-order correlation function, which is defined as

$$g^{(2)}(0) = \frac{\langle a^\dagger a^\dagger a a \rangle}{\langle a^\dagger a \rangle^2}, \quad (13)$$

where the n -th moment can be calculated with P-representation integrals as

$$I_{nn'} = \langle a^\dagger n a^{n'} \rangle = \iint \alpha^{+n} \alpha^{n'} P(\alpha, \alpha^+) d\alpha^+ d\alpha. \quad (14)$$

It is well known that nonclassical effects like photon anti-bunching will occur if $g^{(2)}(0) < 1$ and classical bunching takes place if $g^{(2)}(0) > 1$. Thus, $g^{(2)}(0)$ is often used to distinguish classical from non-classical behavior [33].

The exact solution for the moments [7] is obtained by expanding the term $e^{2\alpha^+ \alpha} = \sum_m 2^m \alpha^m \alpha^{+m} / m!$ in Eq. (11). In this way, we obtain the form of moment after normalization and integration over the complex manifold, as:

$$I_{nn'}^{ex} = N' \sum_m \frac{(2\lambda)^m}{m!} (-\sqrt{\lambda_c})^{n'} (-\sqrt{\lambda_c^*})^n \\ \times {}_2F_1(-m - n', c + 1, 2c + 2, 2) \\ \times {}_2F_1(-m - n, c^* + 1, 2c^* + 2, 2). \quad (15)$$

Here ${}_2F_1$ is the hypergeometric function, and N' is the normalization factor,

$$N'^{-1} = \sum_m \frac{(2\lambda)^m}{m!} {}_2F_1(-m, c + 1, 2c + 2, 2) \\ \times {}_2F_1(-m, c^* + 1, 2c^* + 2, 2). \quad (16)$$

The case of real c has been investigated in Ref [16, 17], where there was no anharmonic nonlinearity, and a real manifold was used. It was suggested that the steady-state distribution approaches a set of δ functions in strong coupling limits. The case without single-photon loss and anharmonic nonlinearity has also been studied in Ref. [34], where one always has $c = -1$. In this case, steady-state Schrödinger cats can be achieved with initial Fock states. Other work studying this potential in different parameter regimes was used to benchmark our numerical results, given below [23].

To understand the physics more clearly, we note that in the limit of $c \rightarrow -1$, the exact solution is a product of simple poles with opposite contour integration directions. These can be integrated using Cauchy's theorem, and correspond to a delta-function solution, so the ratio of the probabilities at the singularities is

$$\frac{P_{ss}(\alpha = \pm\sqrt{\lambda_c}, \alpha^+ = \pm\sqrt{\lambda_c^*})}{P_{ss}(\alpha = \pm\sqrt{\lambda_c}, \alpha^+ = \mp\sqrt{\lambda_c^*})} = e^{4\lambda}, \quad (17)$$

with $\lambda = |\lambda_c|$. If we assume this is also true approximately for $c \neq -1$, we obtain a real distribution [16] in

the form of

$$P_{ss}(\alpha, \alpha^+) = \frac{1}{2(1 + e^{-4\lambda})} \left[\delta(\alpha - \sqrt{\lambda_c}) \delta(\alpha^+ - \sqrt{\lambda_c^*}) \right. \\ \left. + \delta(\alpha + \sqrt{\lambda_c}) \delta(\alpha^+ + \sqrt{\lambda_c^*}) \right] \\ + \frac{1}{2(1 + e^{4\lambda})} \left[\delta(\alpha - \sqrt{\lambda_c}) \delta(\alpha^+ + \sqrt{\lambda_c^*}) \right. \\ \left. + \delta(\alpha + \sqrt{\lambda_c}) \delta(\alpha^+ - \sqrt{\lambda_c^*}) \right]. \quad (18)$$

We now contrast this with an idealized, even cat state $|\psi\rangle_{cat} \propto [|\sqrt{\lambda_c}\rangle + |-\sqrt{\lambda_c}\rangle]$, where the P-representation takes the form after normalization

$$P_{cat}(\alpha, \alpha^+) = \frac{1}{2(1 + e^{-2\lambda})} \left[\delta(\alpha - \sqrt{\lambda_c}) \delta(\alpha^+ - \sqrt{\lambda_c^*}) \right. \\ \left. + \delta(\alpha + \sqrt{\lambda_c}) \delta(\alpha^+ + \sqrt{\lambda_c^*}) \right] \\ + \frac{1}{2(1 + e^{2\lambda})} \left[\delta(\alpha - \sqrt{\lambda_c}) \delta(\alpha^+ + \sqrt{\lambda_c^*}) \right. \\ \left. + \delta(\alpha + \sqrt{\lambda_c}) \delta(\alpha^+ - \sqrt{\lambda_c^*}) \right]. \quad (19)$$

The factor is $e^{-2\lambda}$, rather than $e^{-4\lambda}$ in Eq. (18), so even if the steady state does evolve to a delta-function distribution (18), it will be a mixed state instead of a true cat state. In this case, the density matrix can be derived to have the following form,

$$\rho_{ss} = p |\psi\rangle_{cat} \langle \psi| + (1 - p) \rho_{mix}. \quad (20)$$

Here $p = (1 + e^{2\lambda}) / (1 + e^{4\lambda})$ and $\rho_{mix} = \frac{1}{2} [|\sqrt{\lambda_c}\rangle \langle \sqrt{\lambda_c}| + |-\sqrt{\lambda_c}\rangle \langle -\sqrt{\lambda_c}|]$ is a mixed state. The purity can then be obtained as

$$\mu = Tr [\rho_{ss}^2] = \frac{e^{8\lambda} + 6e^{4\lambda} + 1}{2(e^{4\lambda} + 1)^2}, \quad (21)$$

which is a monotonic decreasing function of λ since

$$\frac{d\mu}{d\lambda} = -\frac{8e^{4\lambda}(e^{4\lambda} - 1)}{(e^{4\lambda} + 1)^3} < 0, \quad (22)$$

for $\lambda > 0$. Thus, the driving will weaken the purity of the steady state since λ is proportional to the driving \mathcal{E}_2 .

It is obvious that we will have $p \rightarrow 1$ in the limit of $\lambda \rightarrow 0$. Thus the delta-function distribution tends to be a true Schrödinger cat state in this limit. However, since $|\lambda_c| = \lambda \rightarrow 0$, the steady state will actually reduce to a vacuum state. This is natural that a non-driven system can be expressed as a vacuum state. In the opposite limit of $\lambda \rightarrow \infty$, the delta-function steady-state distribution (18) will reduce to the mixed state ρ_{mix} since $p \rightarrow 0$. Therefore, a pure Schrödinger cat state is unreachable in the steady state of the system, even using an approximate delta-function solution.

The parity $\hat{\mathcal{P}} = (-1)^{a^\dagger a}$ can also be studied directly with the complex P-distribution (18). In the P-representation, the parity operator is equivalent to the average of $\mathcal{P} = \exp(-2\alpha^+ \alpha)$. In the steady state of the

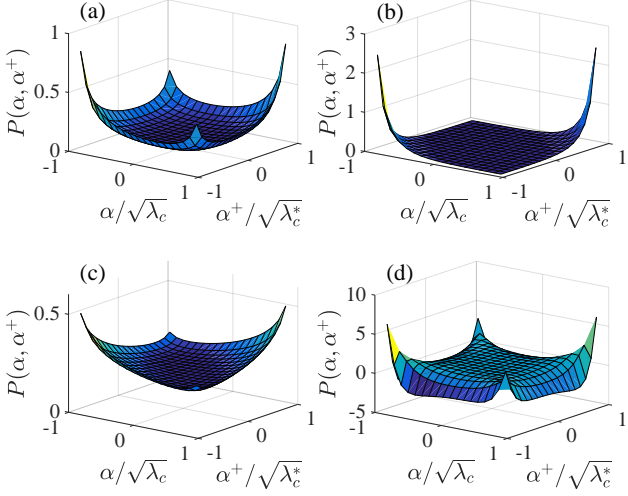


Figure 1. Real parts of steady-state probability distributions (11) for (a) $c = -0.6 - 0.2i$ and $\lambda_c = -0.193 + 0.096i$, (b) large λ : $c = -0.6 - 0.2i$ and $\lambda_c = -1.93 + 0.96i$, (c) small $|Re(c)|$: $c = -0.2 - 0.2i$ and $\lambda_c = -0.193 + 0.096i$, (d) large $|Im(c)|$: $c = -0.6 - 2i$ and $\lambda_c = -0.193 + 0.096i$.

delta-function approximation, we have $\mathcal{P}_{ss} = \text{sech}(2\lambda)$. This means that $\mathcal{P}_{ss} = 1$ in the case of $\lambda = 0$, and $\mathcal{P}_{ss} = 0$ in the limit of $\lambda \rightarrow \infty$. It is consistent with the density matrix (20) which is a vacuum state when $\lambda = 0$ and a mixed state when $\lambda \rightarrow \infty$. The parity is non-conserved because of the nonzero single-photon loss.

The steady-state distributions (11) with different parameters are shown in Fig. 1, plotted on a finite manifold. We see that delta-function distribution will be obtained approximately with large $|Re(c)|$ and small $|Im(c)|$, and reduced to classical mixture of coherent states with large λ . However, these graphs also demonstrate that the probability does not vanish at the boundaries, which means that with $\Re(c) < 0$ on this bounded manifold, the potential solution is no longer a solution to the original master equation, since boundary terms from integration by parts are non-vanishing. An inspection of Fig 1 shows that when assuming a real, bounded manifold, the distribution is neither a true delta function, nor does it vanish at the boundaries, which is the reason why the exact complex contour solution is preferable.

As a result, the true steady states are clearly different to either mixtures of delta functions or Schrödinger cats. This difference can be quantified by using the steady-state distribution (18), to compare moments. The approximate n -th moment is obtained directly with the definition (14) as,

$$I_{nn'}^\delta = \frac{(\sqrt{\lambda_c})^{n'}(\sqrt{\lambda_c^*})^n + (-\sqrt{\lambda_c})^{n'}(-\sqrt{\lambda_c^*})^n}{2(1+e^{-4\lambda})} + \frac{(-\sqrt{\lambda_c})^{n'}(\sqrt{\lambda_c^*})^n + (\sqrt{\lambda_c})^{n'}(-\sqrt{\lambda_c^*})^n}{2(1+e^{4\lambda})}. \quad (23)$$

Similarly, the moment can be written down directly with

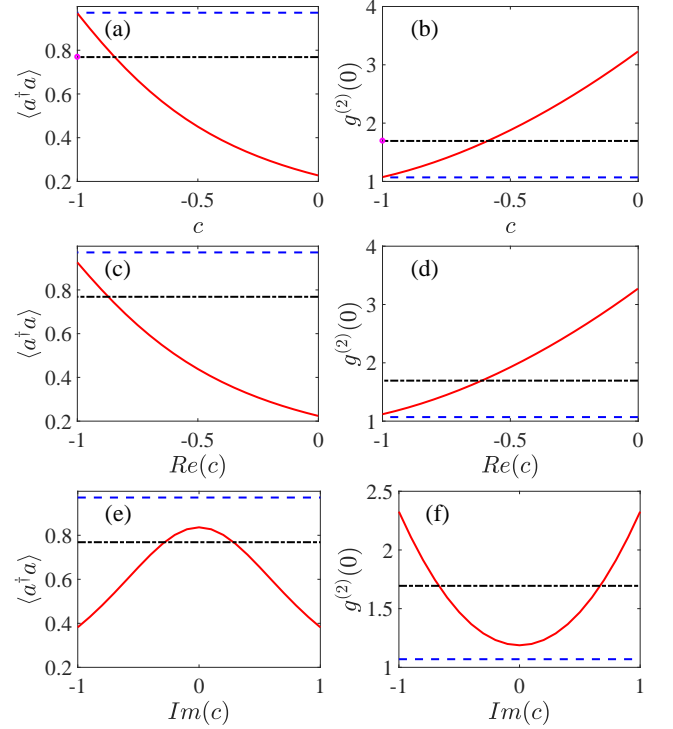


Figure 2. Comparing the average photon numbers (a, c, e) and the second order correlation functions (b, d, f). In figures (a) and (b), they are changing with real c . In figures (c) and (d), they are changing with the real part of c with $Im(c) = -0.2$. In figures (e) and (f), they are changing with the image part of c with $Re(c) = -0.9$. And $\lambda_c = 1 + 0.1i$ in all figures. The blue dashed line is obtained from the delta-function distribution (23), the red solid line from the exact method (15), and the black dash-dotted line from the pure cat state (24). The magenta circles in (a) and (b) are obtained from the results (28) with $\gamma = 0$ exactly and initial vacuum state.

the cat state (19) as:

$$I_{nn'}^{cat} = \frac{(\sqrt{\lambda_c})^{n'}(\sqrt{\lambda_c^*})^n + (-\sqrt{\lambda_c})^{n'}(-\sqrt{\lambda_c^*})^n}{2(1+e^{-2\lambda})} + \frac{(-\sqrt{\lambda_c})^{n'}(\sqrt{\lambda_c^*})^n + (\sqrt{\lambda_c})^{n'}(-\sqrt{\lambda_c^*})^n}{2(1+e^{2\lambda})}. \quad (24)$$

We have compared the average steady-state photon number $\langle a^\dagger a \rangle$ and the second order correlation function $g^{(2)}(0)$ changing with c in Fig. 2. The results of Fig. 2, show that the delta-function distribution (18) is only attainable when $c \rightarrow -1$, which is valid when $\gamma_1^{(1)} \ll \gamma_e^{(2)}$ or $\gamma_1^{(1)} \ll \chi_e$, if there are no detunings. Mathematically, it is obtained by reaching the steady state first and then taking the limit $\gamma_1^{(1)} \rightarrow 0$, which is different from the magenta circles where we take $\gamma_1^{(1)} = 0$ exactly and then get the steady states assuming some particular parity [34]. Number parity is conserved only if $\gamma_1^{(1)} = 0$, and non-conserved if $\gamma_1^{(1)} \neq 0$. Thus the ordering of the limit is

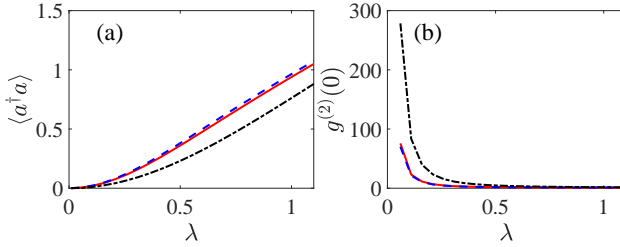


Figure 3. Comparing the average photon number (a) and the second-order correlation function (b) with λ varying. In this case, $c = -0.99 - 0.1i$. The lines have the same meanings as in the Fig. 2.

important, which leads to the gap between the red line with $c \rightarrow -1$ (a mixed state) and the magenta circles (a pure cat state) in Fig. 2. In addition, the delta-function distribution can also be obtainable in the region of extremely strong nonlinearity as the limit $c \rightarrow -1$ suggests, which is more practical than the case $\gamma_1^{(1)} = 0$.

In Fig. 2 the results of the delta-function distributions never agree with those of the cat states. This is consistent with the discussion above that the steady state of the system is always a mixed state (20) instead of a pure cat state. Although there are crosses for the exact results of the steady state and those of the pure cat state, they are always at different c for $\langle a^\dagger a \rangle$ and $g^{(2)}(0)$. The exact steady state is therefore different from both the cat state and a mixture of delta-functions. Hence we can't generate a pure steady-state cat state, unless the system has no single-photon losses.

We have stated that in the limit of small λ , the delta-function distribution (18) tends to an approximate Schrödinger cat. Now we show how $\langle a^\dagger a \rangle$ and $g^{(2)}(0)$ change with λ in Fig. 3. It is natural that the average photon number $\langle a^\dagger a \rangle$ increases with large driving $\mathcal{E}_2 \propto \lambda$ as shown in Fig. 3(a). It also shows that in the region of small λ , their photon numbers agree with each other, but $g^{(2)}(0)$ has a different behavior. This means that even with $\lambda \rightarrow 0$, the delta-function steady-state distribution (18) is still different from the distribution of a Schrödinger cat. We also show in Fig. 3 that in the limit of $c \rightarrow -1$, the exact steady state will approach the delta-function steady-state distribution, although as before, this is not a cat state.

It is directly checked with Eqs. (23) and (24) that the second-order correlation functions are

$$g_\delta^{(2)}(0) = \left(\frac{e^{4\lambda} + 1}{e^{4\lambda} - 1} \right)^2, \quad g_{cat}^{(2)}(0) = \left(\frac{e^{2\lambda} + 1}{e^{2\lambda} - 1} \right)^2. \quad (25)$$

Thus in the limit of $\lambda \rightarrow 0$, we have $g_{cat}^{(2)}(0)/g_\delta^{(2)}(0) \rightarrow 4$. This is consistent with the Fig. 3. In addition, we will also have $g_{cat}^{(2)}(0) > g_\delta^{(2)}(0) > 1$ in all range of λ . This means that their probability distributions are both super-Poissonian [33]. From all the discussions above, we demonstrate that the delta-function steady-state distribution (18) is different from the Schrödinger cat state,

even if $\lambda \rightarrow 0$.

Pure steady-state cats can occur in systems without single-photon loss and anharmonic nonlinearity [34]. If we neglect the single-photon loss in our system from the beginning, the steady-state solution is obtained from solving $\partial\rho_1/\partial t = 0$ in Eq. (6). We expand the density operator in the coherent state basis as $\rho_1(t = \infty) = \sum c_{\alpha,\alpha'} |\alpha\rangle\langle\alpha'| d^2\alpha d^2\alpha'$. Substitute it into Eq. (6) with $\gamma_1^{(1)} = 0$, then for arbitrary $c_{\alpha,\alpha'}$ we have

$$\alpha = \pm\sqrt{\lambda_c}, \quad \alpha' = \pm\sqrt{\lambda_c}. \quad (26)$$

Thus the steady-state density matrix takes the form,

$$\rho_1(\infty) = c_{++} |\sqrt{\lambda_c}\rangle\langle\sqrt{\lambda_c}| + c_{--} |-\sqrt{\lambda_c}\rangle\langle-\sqrt{\lambda_c}| + c_{-+} |-\sqrt{\lambda_c}\rangle\langle\sqrt{\lambda_c}| + c_{+-} |\sqrt{\lambda_c}\rangle\langle-\sqrt{\lambda_c}|, \quad (27)$$

where the coefficients $c_{\alpha,\alpha'}$ are determined by the initial states. This is consistent with the earlier work [34]. In the P-representation, the distribution reads,

$$\begin{aligned} P_\infty(\alpha, \alpha^+) = & c_{++} \delta(\alpha - \sqrt{\lambda_c}) \delta(\alpha^+ - \sqrt{\lambda_c^*}) \\ & + c_{--} \delta(\alpha + \sqrt{\lambda_c}) \delta(\alpha^+ + \sqrt{\lambda_c^*}) \\ & + c_{-+} e^{-2\lambda} \delta(\alpha - \sqrt{\lambda_c}) \delta(\alpha^+ + \sqrt{\lambda_c^*}) \\ & + c_{+-} e^{-2\lambda} \delta(\alpha + \sqrt{\lambda_c}) \delta(\alpha^+ - \sqrt{\lambda_c^*}), \end{aligned} \quad (28)$$

which is also a delta-function distribution. The possible pure state solutions are coherent states and cat states. Since the parity is conserved without single-photon loss according to the master equation (6), Schrödinger cats can be achieved if the initial states are eigenstates of the parity, such as Fock states. The steady-state Schrödinger cats with $\gamma_1^{(1)} = 0$ and initial vacuum states have been obtained in Fig. 2 (a) and (b), where a gap between them and the results related to $\gamma_1^{(1)} \rightarrow 0$ has been observed.

In summary, we have studied the steady states of quantum subharmonic generation with strong nonlinearity, which has been experimental achieved [19]. By comparing the correlation functions, we conclude that true Schrödinger cats cannot survive in the steady state unless there is no single-photon loss. With single-photon loss included, the steady state of the subharmonic generation will reduce to a delta-function steady-state distribution (18) only if there is an extremely strong nonlinearity. More generally, neither type of delta-function solution is obtainable. However, the correct integration manifold is a Pochhammer contour which samples both sheets of a double Riemann sheet contour, intriguingly reflecting some of the character of the known transient macroscopic superposition.

ACKNOWLEDGMENTS

This work is supported by the National Key R&D Program of China (Grants No. 2016YFA0301302 and No. 2018YFB1107200), the National Natural Science Foundation of China (Grants No. 11622428, No. 61475006,

and No. 61675007) and the Graduate Academic Exchange Fund of Peking University. PDD and MDR thank the Australian Research Council and the hospitality of the Institute for Atomic and Molecular Physics (ITAMP)

at Harvard University, supported by the NSF. This research has also been supported by the Australian Research Council Discovery Project Grants schemes under Grants DP180102470 and DP190101480.

[1] E. Schrödinger, *Naturwissenschaften* **23**, 823 (1935).

[2] S. Haroche, *Rev. Mod. Phys.* **85**, 1083 (2013).

[3] D. J. Wineland, *Rev. Mod. Phys.* **85**, 1103 (2013).

[4] M. Arndt and K. Hornberger, *Nat. Phys.* **10**, 271 (2014).

[5] M. Reid and B. Yurke, *Phys. Rev. A* **46**, 4131 (1992).

[6] P. Drummond, K. McNeil, and D. Walls, *Opt. Acta* **27**, 321 (1980).

[7] P. Drummond, K. McNeil, and D. Walls, *Opt. Acta* **28**, 211 (1981).

[8] J. Zhang, P. Hess, A. Kyprianidis, P. Becker, A. Lee, J. Smith, G. Pagano, I.-D. Potirniche, A. C. Potter, A. Vishwanath, *et al.*, *Nature* **543**, 217 (2017).

[9] M. Mirrahimi, Z. Leghtas, V. V. Albert, S. Touzard, R. J. Schoelkopf, L. Jiang, and M. H. Devoret, *New J. Phys.* **16**, 045014 (2014).

[10] S. J. van Enk and O. Hirota, *Phys. Rev. A* **64**, 022313 (2001).

[11] J. Joo, W. J. Munro, and T. P. Spiller, *Phys. Rev. Lett.* **107**, 083601 (2011).

[12] D. S. Simon, G. Jaeger, and A. V. Sergienko, *Phys. Rev. A* **89**, 012315 (2014).

[13] C. Monroe, D. Meekhof, B. King, and D. J. Wineland, *Science* **272**, 1131 (1996).

[14] D. Leibfried, E. Knill, S. Seidelin, J. Britton, R. B. Blakestad, J. Chiaverini, D. B. Hume, W. M. Itano, J. D. Jost, C. Langer, *et al.*, *Nature* **438**, 639 (2005).

[15] A. Ourjoumtsev, H. Jeong, R. Tualle-Brouri, and P. Grangier, *Nature* **448**, 784 (2007).

[16] M. Wolinsky and H. Carmichael, *Phys. Rev. Lett.* **60**, 1836 (1988).

[17] L. Krippner, W. Munro, and M. Reid, *Phys. Rev. A* **50**, 4330 (1994).

[18] W. Munro and M. Reid, *Phys. Rev. A* **52**, 2388 (1995).

[19] Z. Leghtas, S. Touzard, I. M. Pop, A. Kou, B. Vlastakis, A. Petrenko, K. M. Sliwa, A. Narla, S. Shankar, M. J. Hatridge, *et al.*, *Science* **347**, 853 (2015).

[20] F. X. Sun, Q. Y. He, Q. H. Gong, R. Y. Teh, M. D. Reid, and P. D. Drummond, *arXiv:1904.05010* (2019).

[21] P. L. McMahon, A. Marandi, Y. Haribara, R. Hamerly, C. Langrock, S. Tamate, T. Inagaki, H. Takesue, S. Utsunomiya, K. Aihara, *et al.*, *Science* **354**, 614 (2016).

[22] P. D. Drummond and P. Kinsler, *Phys. Rev. A* **40**, 4813 (1989).

[23] N. Bartolo, F. Minganti, W. Casteels, and C. Ciuti, *Phys. Rev. A* **94**, 033841 (2016).

[24] P. Drummond and D. Walls, *J. Phys. A* **13**, 725 (1980).

[25] P. Drummond and C. Gardiner, *J. Phys. A* **13**, 2353 (1980).

[26] R. Graham and H. Haken, *Z. Phys. A* **243**, 289 (1971).

[27] R. Graham and H. Haken, *Z. Phys. A* **245**, 141 (1971).

[28] H. Risken, *Z. Phys. A* **251**, 231 (1972).

[29] K. Seybold and H. Risken, *Z. Phys.* **267**, 323 (1974).

[30] L. Pochhammer, *Mathematische Annalen* **35**, 495 (1890).

[31] T. M. MacRobert, *Functions of a Complex Variable*, Vol. 1954 (Macmillan, 1938).

[32] H. Bateman, *Higher transcendental functions* (McGraw-Hill, New York, 1955).

[33] M. O. Scully and M. S. Zubairy, *Quantum Optics* (Cambridge University Press, 1997).

[34] L. Gilles, B. Garraway, and P. Knight, *Phys. Rev. A* **49**, 2785 (1994).